Research Article Vol. 32, No. 7 / 25 Mar 2024 / Optics Express 11395

Optics EXPRESS

Turbulence-resistant free space optical communication via chaotic block-matching and 3D filtering

TINGWEI WU,[1,2,3] HANXIANG MOU,[1,2] YUTONG HE,[4] YEJUN LIU,[1,2,*] SONG SONG,[1,2] LUN ZHAO,[1,2] AND LEI GUO[1,2]

[1] *School of Communications and Information Engineering, Chongqing University of Posts and Telecommunications, Chongqing 400065, China*
[2] *Institute of Intelligent Communication and Network Security, Chongqing University of Posts and Telecommunications, Chongqing 400065, China*
[3] *Postdoctoral Research Workstation of Chongqing Key Laboratory of Cyberspace and Information Security, School of Security and Information Law, Chongqing University of Posts and Telecommunications, Chongqing, China*
[4] *Southwest Institute of Technical Physics, Chengdu 610041, China*
[*] *yjliu@cqupt.edu.cn*

Abstract: In this paper, we propose a chaotic block-matching and three-dimensional (C-BM3D) filtering algorithm to remove the noise and enhance the security in the turbulent channel of free space optical (FSO) communication. We experimentally demonstrate the performance of C-BM3D by comparing it with chaotic non-local means filtering (C-NLM), chaotic Gaussian filtering and chaotic Median filtering based on Log-normal and Gamma-Gamma turbulence models. The results show that the peak signal-to-noise ratios (PSNRs) of C-BM3D in the weak turbulence under Log-normal and Gamma-Gamma models are up to 96.2956 and 93.2853, respectively. The C-BM3D also achieves superior image similarity in Log-normal turbulent channel, with its structural similarity index measures (SSIMs) nearly equal to 1. Additionally, the signal-to-noise ratio (SNR) of C-BM3D ranks the highest, and its bit error rate (BER) improves by at least 15 dB compared to that of the other three algorithms. The experimental results indicate that the C-BM3D can be a good candidate for the next generation of FSO communication in security and turbulence resistance.

1. Introduction

Free space optical (FSO) communication has been widely applied to low earth orbit (LEO) satellite, underwater and unmanned aerial vehicle (UAV) communications because of its license-free, easy deployment, high capacity, etc. For example, C. Li et al. studied a wavelength-division-multiplexing (WDM) four-level pulse amplitude modulation (PAM4) FSO-underwater wireless optical communication (UWOC) integrated system based on 100 Gb/s channel capacity [1]. Since FSO systems do not require license fees, FSO has been viewed as an alternative technology to conventional radiofrequency (RF) systems [2–4] in geostationary satellites [5–7]. To further improve the FSO communication performance, relay-assisted FSO system has been proposed in [8], which outperforms the pure FSO system. FSO links [9] achieve robust and low-latency communications between autonomous underwater vehicle (AUV) and UAV. Authors in [10] also combined UAV with dual-hop RF/FSO relay system to achieve extensive and reliable communications in space-air-ground integrated networks (SAGIN).

However, turbulence is one of the main factors that adversely influences the performance of FSO communication. If a laser transmits through turbulence, intensity fluctuation and optical power attenuation exist, which affects communication performance in turn [11]. There have been many studies about transmitting general information in FSO channels [12–15], which achieved

#511548 https://doi.org/10.1364/OE.511548
Journal © 2024 Received 9 Nov 2023; revised 7 Feb 2024; accepted 29 Feb 2024; published 13 Mar 2024

great progress in resisting turbulence. However, there is little research on FSO image transmission. The previous experiments of traditional Gaussian filtering [16] and Median filtering [17] verified that although they have good denoising effects, they are at the expense of communication quality in FSO transmission. The newly proposed non-local means (NLM) filtering [18] can make full use of redundant information and maintain the details of the image, but the noise of similar blocks increases when searching for weights. Based on the above reduction methods, block-matching and three-dimensional (BM3D) filtering is proposed [19] to combine the spatial and frequency domain algorithms, which achieves better visual effects and higher similarity. The latest studies [20–23] show that, compared with traditional filtering algorithms, two-step iterative shrink/threshold segmentation and enhanced Lagrange algorithm, the introduction of the BM3D algorithm not only improves the image reconstruction quality but also enhances the anti-noise capability of the technique.

Due to the exposure of optical signals in FSO communication, the transmitted signals are prone to be eavesdropped and accessed by illegal attackers [24]. The chaotic technique has been widely used in image encryption [25] and security enhancement [26,27] of fiber optic communication thanks to its high sensitivity to initial values, strong unpredictability, etc. For instance, WDM signals can achieve secure transmission on 50 km standard single-mode optical fiber using the private chaotic phase in disarray [28]. Chaotic compressive sensing (CS) successfully enhances the orthogonal frequency division multiplexing-passive optical network (OFDM-PON) transmission security [29]. Chaotic three-dimensional (3D) constellation scrambling could effectively enhance the security and transmission performance of coherent optical orthogonal frequency-division multiplexing (CO-OFDM) systems [30].

In this paper, we combine logistic chaotic mapping with the BM3D filtering algorithm to resist the turbulence and enhance the security of FSO communication. Specifically, the image is encrypted at the transmitter by digital chaos and decrypted at the receiver. At the receiver, the image with turbulence will be filtered by the C-BM3D and other typical filtering algorithms. To clarify the superiority of C-BM3D, we will compare the bit error rate (BER), structural similarity index measure (SSIM) and peak signal-to-noise ratio (PSNR) performance of different filtering algorithms in different turbulent conditions.

2. Principle

2.1. Atmospheric turbulence in FSO channels

Among common statistical models for simulating turbulent conditions, the Log-normal and Gamma-Gamma models are widely used to study turbulence-resistant techniques [31]. The probability distribution function (PDF) of Log-normal is expressed as [32]:

$$p(I) = \frac{1}{\sqrt{2\pi\sigma_l^2}}\frac{1}{I}\exp(-\frac{(In(\frac{1}{I_0}+\frac{\sigma_l^2}{2}))^2}{2\sigma_l^2}), \tag{1}$$

where I is the irradiance intensity in turbulent medium, I_0 is the irradiance intensity in free space, $\sigma^2 l$ is log irradiance variance that represents the strength of atmospheric turbulence. The PDF of Gamma-Gamma is expressed as:

$$f_{\gamma_b}(\gamma_b) = \frac{\alpha\beta^{(\alpha+\beta)/2}\bar{\gamma}_b^{-(\alpha+\beta)/4}}{\Gamma(\alpha)\Gamma(\beta)}\gamma_b{}^{-(\alpha+\beta)/4-1} \times K_{\alpha-\beta}[2\sqrt{\alpha\beta\sqrt{\frac{\gamma_b}{\bar{\gamma}_b}}}], \tag{2}$$

where $\Gamma(.)$ represents the Gamma function, and K_n (.) is the modified Bessel function of the second kind of order n. The $\bar{\gamma}_b$ is average signal-to-noise ratio (SNR) per bit, given by $\bar{\gamma}_b = E[A^2]E_b/N_0$. The α and β are given by (3) and (4), which are shaping parameters that are

Optics EXPRESS

related to the effective number of large-scale and small-scale eddies in the scattering process, respectively.

$$\alpha = [\exp(\frac{0.49\sigma_R^2}{(1+1.11\sigma_R^{12/5})^{5/6}}) - 1]^{-1}, \tag{3}$$

$$\beta = [\exp(\frac{0.51\sigma_R^2}{(1+0.69\sigma_R^{12/5})^{5/6}}) - 1]^{-1}, \tag{4}$$

where σ_R is the Rytov variance, namely the intensity of turbulence.

2.2. Logistic chaotic mapping

Logistic mapping is a typical nonlinear iterative equation, as shown in the equation:

$$x_{k+1} = \mu \times x_k(1 - x_k), k = 0, 1, \cdots\cdots, n, \tag{5}$$

where μ is the control parameters, $\mu \in (0, 3.5699456]$, x_k is the chaotic sequence, $x_0 \in (0, 1)$, and k is the iteration time step.

One main characteristic of chaotic systems is the high initial sensitivity. When $\mu =$ 0.190903252535798, $x_1 = 0.699076722656686$, $x_2 = 0.699076722656687$, the initial sensitivity of the logistic chaotic mapping is shown in Fig. 1. After certain iterations, the mixed chaotic sequence splits into two sequences with different translations. As the number of iterations increases, the values of the two sequences show bigger difference. It shows that the chaotic system still maintains the initial value sensitivity of logistic chaotic mapping.

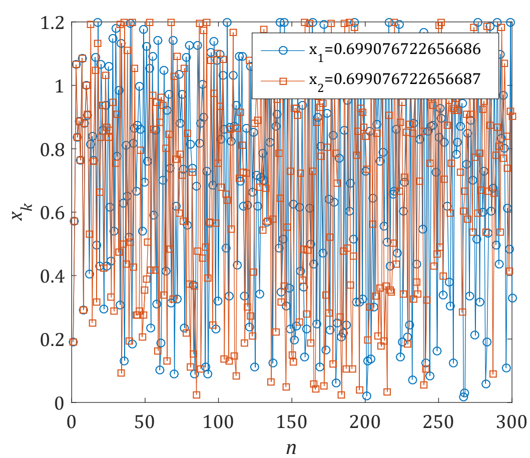

Fig. 1. Initial value sensitivity.

2.3. BM3D algorithm

BM3D algorithm [33] can find similar blocks to reference blocks of two-dimensional (2D) images. It stacks 2D-image similar blocks into 3D groups, which can be performed by collaborative filtering. We estimate the recovered image by aggregating the processed results and original image blocks. The overall process of the algorithm is shown in Fig. 2, which can be divided into two steps: Hard-thresholding filtering and Wiener filtering.

We use Z_x to represent a square block of $N_1 \times N_1$ on the noisy image z with the top-left coordinate x. $x \in X$, X is the image domain. Z_s is a 3D block, and the top-left coordinates of all

Optics EXPRESS

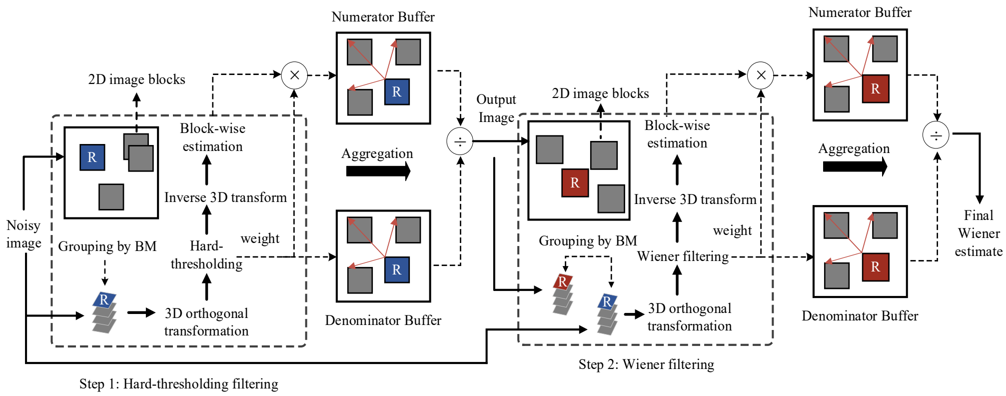

Fig. 2. Execution process of BM3D and the reference block is marked with "R".

2D blocks are defined by the set S. To represent the reference block in each 3D block, we add the R (reference block) identifier under the corresponding coordinate, namely x_R. Similarly, we use Y_x to represent a block on a noiseless image y. Because Step1 and Step2 are the same structure, the meanings of some parameters are also the same. In order to distinguish the parameters in the two steps, we add the "*ht*" and "*wie*" marks, respectively. For the basic estimation image of Step1, we use $\hat{y}^{basic}$ to represent it, and the final estimation image obtained by Step2 is $\hat{y}^{final}$.

1. Basic estimates: Hard-thresholding filtering

   (1) Estimates by block: For each block of the noisy image:

   a) Grouping. After finding similar blocks to the reference block, they are altogether stacked into a 3D array. When the noise variance is large or the block is relatively small, it is not accurate to find similar blocks based on the noisy image z. Therefore, the two blocks on the noisy image z are separated by 2D normalized transformation. Then, the coefficients whose amplitude is less than a certain threshold are set to zero, so that the matching error of the two blocks can be expressed as the mean square error of these coefficients.

$$d(Z_{x_R}, Z_x) = \frac{||\gamma'(\tau_{2D}^{ht}(Z_{x_R})) - \gamma'(\tau_{2D}^{ht}(Z_x))||_2^2}{(N_1^{ht})^2}, \tag{6}$$

   where γ' is a hard threshold operator with threshold $\lambda_{2D}\sigma$, $||.||^2{}_2$ is the 2-norm, N_1^{ht} is the block size used in basic estimates, τ_{2D}^{ht} is the 2D normalized transformation.

   After calculating the matching error between the current reference block and all other blocks according to Eq. (6), we only keep those blocks whose error is less than a certain threshold and get the corresponding coordinate set:

$$S_{x_R}^{ht} = \{x \in X : d(Z_{x_R}, Z_x) \leq \tau_{match}^{ht}\}, \tag{7}$$

   where τ_{match}^{ht} is the maximum error threshold for determining the similarity of two blocks, which is generally set according to experience. The current reference block will be judged to be a similar block because its matching error is 0, so there is at least one element in the coordinate set. By stacking all the similar blocks together, we get a 3D array $Z_{S_{xR}^{ht}}$ of shape $N_1^{ht} \times N_1^{ht} \times |S_{x_R}^{ht}|$, where $|S_{x_R}^{ht}|$ represents the number of elements in the collection.

   b) Collaborative hard thresholding. After obtaining the 3D array corresponding to the reference block, we can carry out 3D collaborative transformation and filtering, which can

Optics EXPRESS

be formally expressed as (8). Firstly, the 3D normalized transformation is applied to the above groups. After obtaining the non-zero component from the weight coefficient by hard threshold, the inverse 3D normalized transformation is performed to get the estimation of all grouped blocks. Finally, they are returned to their original positions.

$$\hat{Y}^{ht}_{S^{ht}_{x_R}} = \tau^{ht\ -1}_{3D}(\gamma(\tau^{ht}_{3D}(Z_{S^{ht}_{x_R}}))), \tag{8}$$

where γ is a hard threshold operator with threshold $\lambda_{3D}\sigma$, $Z_{S^{ht}_{x_R}}$ is the formed 3D groups, τ^{ht}_{3D} is the 3D normalized transformation and $\tau^{ht\ -1}_{3D}$ is the inverse 3D normalized transformation.

(2) Aggregation: The superposition weights are calculated by the number of non-zero components. Finally, the estimated image is obtained by dividing the superimposed blocks by the weights of each block.

$$\hat{y}^{basic}(x) = \frac{\sum\limits_{x_R \in X} \sum\limits_{x_m \in S^{ht}_{x_R}} \omega^{ht}_{x_R} \hat{Y}^{ht,x_R}_{x_m}(x)}{\sum\limits_{x_R \in X} \sum\limits_{x_m \in S^{ht}_{x_R}} \omega^{ht}_{x_R} \chi_{x_m}(x)}, \forall x \in X. \tag{9}$$

We assume that each block has been filled to the same size as the original image by zeros and $\chi_{x_m} : X \longrightarrow \{0, 1\}$ is used to determine whether a pixel x is on block x_m.

2. Final estimates: Wiener Filtering

(1) Estimates by block: For each block of the obtained image from basic estimates:

a) Grouping. Within the basic estimates range, block matching (BM) is used to find the location of all blocks that are similar to the reference block, namely R. In this section, we find similar blocks by (10) based on the basic estimation image. Because the current noise is relatively small, it is not necessary to do transformation and hard-thresholding like (6).

$$S^{wie}_{x_R} = \left\{ x \in X : \frac{||\hat{Y}^{basic}_{x_R} - \hat{Y}^{basic}_{x}||^2_2}{(N^{wie}_1)^2} < \tau^{wie}_{match} \right\}, \tag{10}$$

where N^{wie}_1 is the block size used in Wiener filtering, τ^{wie}_{match} is the maximum d-distance for which two blocks are considered similar, $\hat{Y}^{basic}_{x_R}$ and $\hat{Y}^{basic}_{x}$ are the basic estimate blocks located at x_R and x, respectively. Now there are two groups formed, one from the noisy image and another one from the basic estimates: $\hat{Y}^{wie}_{S^{wie}_{xR}}$ and $Z_{S^{wie}_{xR}}$. $\hat{Y}^{wie}_{S^{wie}_{xR}}$ is obtained by stacking together the basic estimate blocks $\hat{Y}^{basic}_{x \in S^{wie}_{x_R}}$, and $Z_{S^{wie}_{xR}}$ is obtained by stacking together the noisy blocks $Z_{x \in S^{wie}_{x_R}}$.

b) Collaborative Wiener filtering. The 3D normalized transformation is applied to the above two groups. The Wiener filtering is performed on the noisy one. Next, the inverse 3D normalized transformation is applied to the filtered Wiener shrinkage coefficients to estimate all blocks. Finally, these block estimates are returned to their original positions. The estimates are shown as:

$$\hat{Y}^{wie}_{S^{wie}_{x_R}} = \tau^{wie^{-1}}_{3D}(W_{S^{wie}_{x_R}} \tau^{wie}_{3D}(Z_{S^{wie}_{x_R}})), \tag{11}$$

where $W_{S^{wie}_{x_R}}$ is the Wiener shrinkage coefficient, $Z_{S^{wie}_{x_R}}$ is the noisy blocks in final estimates.

(2) Aggregation: The final estimate $\hat{y}^{final}(x)$ of the real image is calculated by aggregating all the obtained local estimates using the weighted average.

$$\hat{y}^{final}(x) = \frac{\sum\limits_{x_R \in X} \sum\limits_{x_m \in S_{x_R}^{wie}} \omega_{x_R}^{wie} \hat{Y}_{x_m}^{wie,x_R}(x)}{\sum\limits_{x_R \in X} \sum\limits_{x_m \in S_{x_R}^{wie}} \omega_{x_R}^{wie} \chi_{x_m}(x)}, \forall x \in X. \tag{12}$$

3. Simulation process and analysis

In this experiment, we aim to simulate and verify the denoising effect and communication quality of the C-BM3D algorithm by comparing it with the C-NLM algorithm, chaotic Gaussian filtering and chaotic Median filtering under Log-normal and Gamma-Gamma turbulence models. Specifically, the matrix size of the experimental image is 256×256. Firstly, the image is encrypted by logistic chaotic mapping. The logistic map is used to generate an array of sequence of random numbers. After obtaining random sequence, the image is cluttered and diffused at the bit plane. Finally, the bitstream of 1*65536 is got by XOR operation on the random image and the random sequence by bit, which is transmitted through the FSO channel. The decryption process is the reverse of encryption. At the receiver, the image recovered from the received bitstream will be filtered by C-BM3D, C-NLM, chaotic Gaussian filtering and chaotic Median filtering. The experimental FSO communication system is shown in Fig. 3, and the simulation parameters are listed in Table 1.

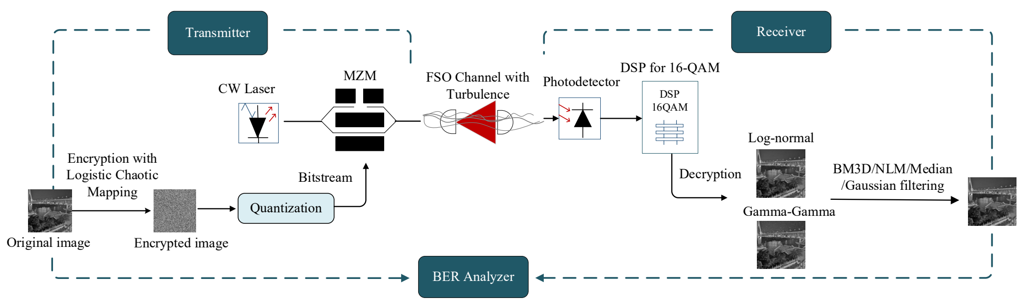

Fig. 3. The experimental FSO communication system.

Table 1. The simulation parameters

Parameter	Value
Wavelength	1550 nm
Beam divergence	2 mrad
Transmitter aperture diameter	5 cm
Receiver aperture diameter	20 cm
Range	1 km
Attenuation	5~15 dB/km
Scintillation model	Log-normal/Gamma-Gamma
Refractive index structure ($c^2{}_n$)	10^{-15} m$^{-2/3}$~10^{-13} m$^{-2/3}$

Additionally, we calculate the SNR and BER to evaluate the communication quality after the four algorithms. And we calculate the PSNR and SSIM of the recovered image and original image to judge the image quality. The formulas are as:

$$SNR = 10 * \log_{10}(Ps/Pn) \tag{13}$$

where Ps represents the average power of the signal and Pn represents the average power of the noise.

$$P_b = I_e/I, \tag{14}$$

where I_e represents the number of bits accepted in error, and I represents the total number of transmitted bits.

$$PSNR(f,g) = 10\lg \frac{(2^n - 1)^2}{\sum\limits_i \sum\limits_j \frac{(f(i,j)-g(i,j))^2}{MN}}, \tag{15}$$

where $f(i,j)$ is the original image, $g(i,j)$ is the restored image. i and j are the image pixels. $M \times N$ is the image size.

$$SSIM(f,g) = \frac{(2\mu_f\mu_g + c_1)(2\sigma_{fg} + c_2)}{(\mu_f^2 + \mu_g^2 + c_1)(\sigma_f^2 + \sigma_g^2 + c_2)}, \tag{16}$$

where μ_f is the mean value of f and μ_g is the mean value of g. $\sigma^2{}_f$ is the variance of f and $\sigma^2\, g$ is the variance of g. σ_{fg} is the covariance of f and g. $c_1 = (k_1 L)^2$ and $c_1 = (k_1 L)^2$ are two constants to avoid division by zero. The closer the SSIM value is to 1, the higher similarity between the original image and the recovered image.

3.1. Image quality under turbulence of different intensity

In this section, we aim to compare the PSNR and SSIM of filtering algorithms to estimate the image quality under Log-normal and Gamma-Gamma turbulence models by combining Opti-System with MATLAB. The experiment will be carried out in three different intensities of turbulence in each model: weak, moderate and strong. The values of attenuation (a) are set at 5 dB, 12 dB, 15 dB, respectively, and the values of index refraction structure ($c^2{}_n$) are set at $8 \times 10^{-15}\mathrm{m}^{-2/3}$, $3 \times 10^{-14}\mathrm{m}^{-2/3}$, $1 \times 10^{-13}\mathrm{m}^{-2/3}$, respectively. The results of Log-normal and Gamma-Gamma turbulence models are illustrated in Table 2 and Table 3, respectively. From the data in the two tables below, the PSNRs of C-BM3D in weak turbulence under Log-normal and Gamma-Gamma models are up to 96.2956 and 93.2853, respectively, which are much higher than that of the other three algorithms. Furthermore, C-BM3D and chaotic Gaussian filtering achieve superior image similarity in the Log-normal turbulent channel, with their SSIMs nearly equal to 1. However, it is also apparent that the PSNRs of C-BM3D in strong turbulence under the Gamma-Gamma model present dramatic decrease, even as low as 26.0561. Under strong turbulence, the noise is so dense that the similar blocks may contain some noise. The denoising effect decreases with the estimation error increases. For chaotic Median filtering and C-NLM, their values do not experience obvious change, which have been kept at lower numbers than C-BM3D and chaotic Gaussian filtering. Overall, these results indicate that the C-BM3D has good image denoising and reconstruction performance, with its higher PSNRs and SSIMs in Log-normal and Gamma-Gamma turbulent channels.

3.2. Communication quality under turbulence of different intensity

In this section, we demonstrate the SNR distribution of filtering algorithms to estimate their communication quality under the Gamma-Gamma turbulence model (Since C-BM3D has already shown superior PSNR performance in the Log-normal turbulent channel from the former section). The experiment will be carried out in four different intensities of turbulence, as shown in Fig. 4. The values of a are set at 5 dB, 10 dB, 12 dB and 15 dB, respectively, and the values of $c^2{}_n$ are set at $8 \times 10^{-15}\mathrm{m}^{-2/3}$, $8 \times 10^{-14}\mathrm{m}^{-2/3}$, $8 \times 10^{-13}\mathrm{m}^{-2/3}$ and $8 \times 10^{-12}\,\mathrm{m}^{-2/3}$, respectively. It is

Table 2. Comparison in Log-normal Turbulent Channel

		C-Median	C-NLM	C-BM3D	C-Gaussian
PSNR	Weak	29.6564	32.4555	96.2956	36.1032
	Moderate	26.9869	29.6025	71.2036	36.1028
	Strong	26.9658	29.0344	33.2884	33.5285
SSIM	Weak	0.8872	0.8937	1.0000	0.9789
	Moderate	0.8006	0.8230	1.0000	0.9747
	Strong	0.7885	0.8092	0.9555	0.9481

Table 3. Comparison in Gamma-Gamma Turbulent Channel

		C-Median	C-NLM	C-BM3D	C-Gaussian
PSNR	Weak	26.9878	29.6024	93.2853	36.1032
	Moderate	26.9717	29.3614	36.0765	34.5647
	Strong	26.8653	25.8740	26.0561	28.8840
SSIM	Weak	0.8006	0.8230	1.0000	0.9747
	Moderate	0.7999	0.8167	0.9741	0.9592
	Strong	0.7956	0.7167	0.8043	0.8511

obvious from Fig. 4 that the SNR of C-BM3D has ranked the highest, even peaking at over 100, while the SNRs of other algorithms have kept at less than 40. Thus, C-BM3D has greater advantages in improving communication quality in FSO communication. However, it can also be seen that C-BM3D shows inferior stability when it comes to strong turbulence under the Gamma-Gamma model.

To further verify the performance of C-BM3D and logistic chaotic mapping, we calculate the BER distribution of the BM3D, NLM, Gaussian filtering, Median filtering and FSO channel with and without chaos, as shown in Fig. 5. Specifically, Fig. 5(a) and Fig. 5(b) demonstrate the results under Log-normal and Gamma-Gamma turbulence models, respectively. It can be seen from Fig. 5 that the BER difference between with and without chaos of every algorithm is little, indicating that logistic chaotic mapping has no adverse effect on the FSO communication quality but also improves communication security. Importantly, the BER values of the BM3D algorithm and FSO channel are almost equal, indicating that the BM3D algorithm improves the image quality without sacrificing the communication quality. From Fig. 5(a), the BM3D algorithm improves at least 24 dB BER performance than the other three algorithms in Log-normal turbulent condition. The superiority of the BM3D algorithm is also verified under the Gamma-Gamma turbulence model. From Fig. 5(b), the BER value of the BM3D algorithm remains unchanged at approximately 0.014 in weak turbulence of the Gamma-Gamma model, improving by at least 15 dB compared with other algorithms. Thus, the BM3D algorithm improves the image quality and communication quality greatly, which can be a good candidate for the next generation of FSO communication in security and turbulence resistance.

Optics EXPRESS

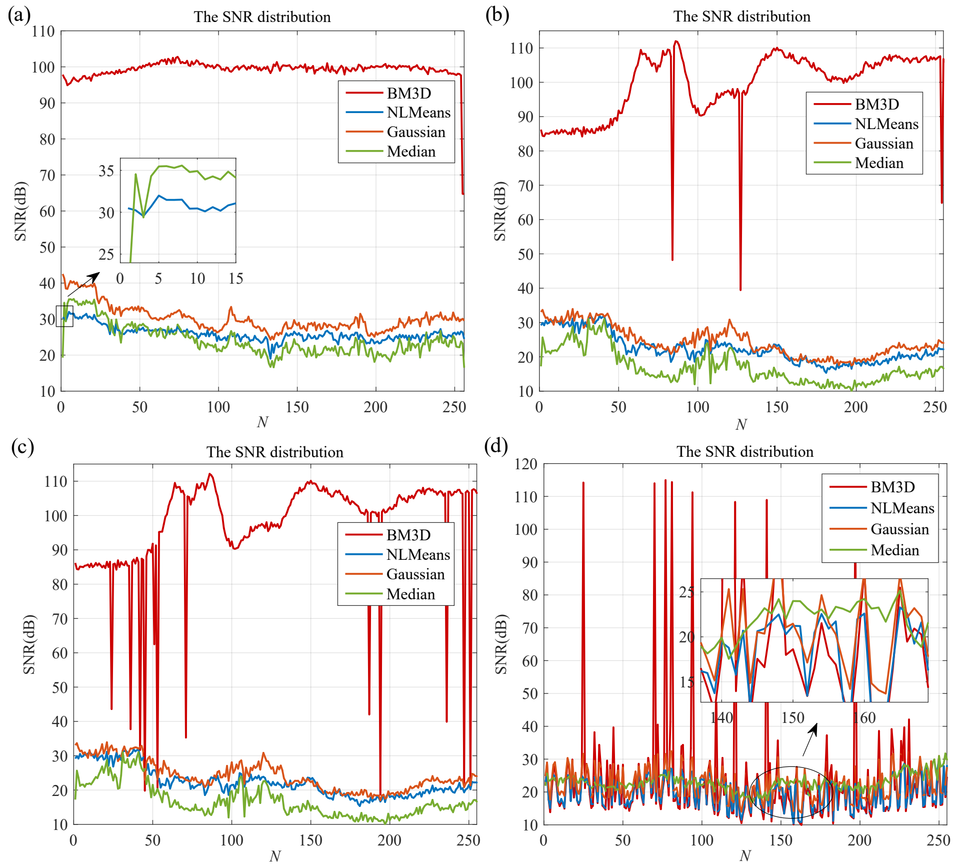

Fig. 4. The SNR distribution of C-NLM, C-BM3D, chaotic Gaussian filtering, chaotic Median filtering under different Gamma-Gamma turbulent conditions: (a) $a = 5$ dB/km, $c_n^2 = 8 \times 10^{-15} m^{-2/3}$; (b) $a = 10$ dB/km, $c_n^2 = 8 \times 10^{-14} m^{-2/3}$; (c) $a = 12$ dB/km, $c_n^2 = 8 \times 10^{-13} m^{-2/3}$; (d) $a = 15$ dB/km, $c_n^2 = 8 \times 10^{-12} m^{-2/3}$.

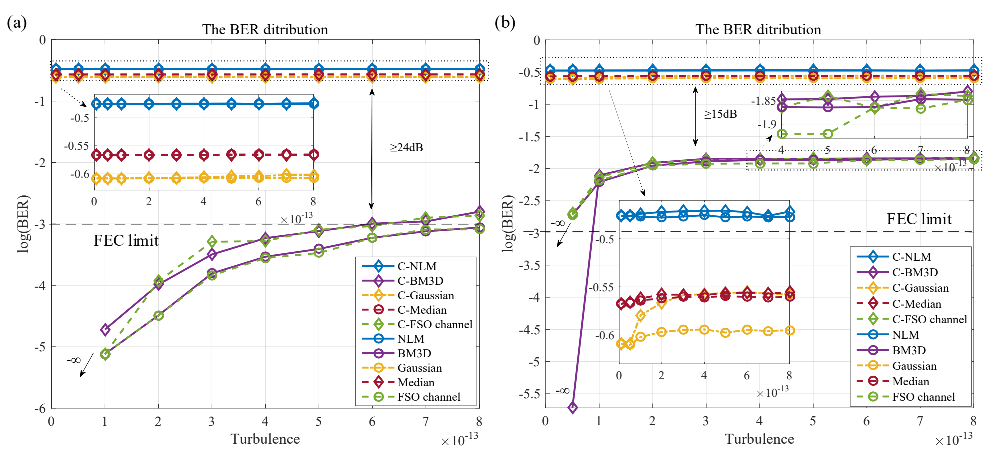

Fig. 5. The BER distribution of C-NLM, C-BM3D, chaotic Gaussian filtering, chaotic Median filtering under Log-normal (a) and Gamma-Gamma (b) turbulent conditions.

4. Conclusion

In this paper, we compare the communication performance of C-BM3D, C-NLM, chaotic Gaussian filtering and chaotic Median filtering under Log-normal and Gamma-Gamma turbulence models in the FSO system. The results show that the PSNRs of C-BM3D in the weak turbulence under Log-normal and Gamma-Gamma models are up to 96.2956 and 93.2853, respectively. The C-BM3D also achieves superior image similarity in the Log-normal turbulent channel, with its SSIMs nearly equal to 1. Additionally, the SNR of C-BM3D has ranked the highest, and its BER has remained at the lowest among the four algorithms in FSO communication, improving at least 15 dB BER performance compared with other algorithms. Overall, C-BM3D outperforms other methods since it not only recovers the image with superior quality from the chaotic system of the FSO communication system but also enhances communication quality and security. However, one problem is that the C-BM3D lacks stability in strong turbulence, which needs to be further improved and studied in the future.

Funding. National Natural Science Foundation of China (62025105, 62301097, U21B2005); China Postdoctoral Science Foundation (2023T160775); Natural Science Foundation of Chongqing (CSTB2022NSCQ-MSX0542); Chongqing Municipal Education Commission (KJQN202200610).

Disclosures. The authors declare no conflicts of interest.

Data availability. The original contributions presented in the study are included in the article, further inquiries can be directed to the corresponding author.

References

1. C. Y. Li, X. H. Huang, H. H. Lu, *et al.*, "A WDM PAM4 FSO–UWOC integrated system with a channel capacity of 100 Gb/s," J. Lightwave Technol. **38**(7), 1766–1776 (2020).
2. Z. Hu, C. Chen, Z. Zhang, *et al.*, "Secure Cooperative Transmission for Mixed RF/FSO Spectrum Sharing Networks," IEEE Trans. Commun. **68**(5), 3010–3023 (2020).
3. S. Malik, P. Saxena, and Y. H. Chung, "Performance analysis of a UAV-based IRS-assisted hybrid RF/FSO link with pointing and phase shift errors," J. Opt. Commun. Netw. **14**(4), 303–315 (2022).
4. Z. Zhang, Q. Sun, M. López-Benítez, *et al.*, "Performance Analysis of Dual-Hop RF/FSO Relaying Systems With Imperfect CSI," IEEE Trans. Veh. Technol. **71**(5), 4965–4976 (2022).
5. Y. Ma, T. Lv, G. Pan, *et al.*, "On secure uplink transmission in hybrid RF-FSO cooperative satellite-aerial-terrestrial networks," IEEE Trans. Commun. **70**(12), 8244–8257 (2022).
6. Q. Huang, M. Lin, W. P. Zhu, *et al.*, "Uplink Massive Access in Mixed RF/FSO Satellite-Aerial-Terrestrial Networks," IEEE Trans. Commun. **69**(4), 2413–2426 (2021).
7. E. Zedini, A. Kammoun, and M. S. Alouini, "Performance of multibeam very high throughput satellite systems based on FSO feeder links with HPA nonlinearity," IEEE Trans. Commun. **19**(9), 5908–5923 (2020).
8. G. Xu, Q. Zhang, Z. Song, *et al.*, "Relay-Assisted Deep Space Optical Communication System Over Coronal Fading Channels," IEEE Trans. Aerosp. Electron. Syst. **59**(6), 8297–8312 (2023).
9. P. Agheli, H. Beyranvand, and M. J. Emadi, "UAV-assisted underwater sensor networks using RF and optical wireless links," J. Lightwave Technol. **39**(22), 7070–7082 (2021).
10. L. Qu, G. Xu, Z. Zeng, *et al.*, "UAV-Assisted RF/FSO Relay System for Space-Air-Ground Integrated Network: A Performance Analysis," IEEE Trans. Wireless Commun. **21**(8), 6211–6225 (2022).
11. M. K. Miao and X. F. Li, "Performance analysis of FSO systems over a Lognormal-Rician turbulence channel with generalized pointing errors," J. Lightwave Technol. **40**(13), 4206–4216 (2022).
12. T. W. Wu, W. Zeng, Y. J. Liu, *et al.*, "Secure turbulence-resistant coherent free-space optical communications via chaotic region-optimized probabilistic constellation shaping," Opt. Lett. **48**(3), 684–687 (2023).
13. L. B. Stotts and L. C. Andrews, "Adaptive optics model characterizing turbulence mitigation for free space optical communications link budgets," Opt. Express **29**(13), 20307–20321 (2021).
14. Y. T. Huang, H. Z. Huang, H. S. Chen, *et al.*, "Free-space optics communications employing elliptical-aperture multimode diversity reception under anisotropic turbulence," J. Lightwave Technol. **40**(5), 1502–1508 (2022).
15. C. Qiu, W. Q. Ma, F. Wang, *et al.*, "Atmospheric turbulence resistant heterodyne coherent receiver of few-mode fiber," Opt. Express **30**(16), 28312–28324 (2022).
16. A. K. Singh, "Major development under Gaussian filtering since unscented Kalman filter," IEEE/CAA J. Autom. Sinica **7**(5), 1308–1325 (2020).
17. Q. Wang, K. Zhao, X. Yi, *et al.*, "Low-cost OFDR distributed sensing based on optical fiber with enhanced rayleigh backscattering profiles and Median filtering," in *27th International Conference on OFS* (Optica Publishing Group, 2022), paper Th4.48.
18. M. F. Wu, Y. F. Chen, P. B. Zhu, *et al.*, "NLM parameter optimization for ϕ -OTDR signal," J. Lightwave Technol. **40**(17), 6045–6051 (2022).

Optics EXPRESS

19. Y. H. Do, Y. Cho, S. H. Kang, *et al.*, "Optimization of block-matching and 3D filtering (BM3D) algorithm in brain SPECT imaging using fan beam collimator: Phantom study," Nucl. Eng. Technol. **54**(9), 3403–3414 (2022).
20. M. Pan, P. D. Hua, Z. Y. Ding, *et al.*, "Long distance distributed strain sensing in OFDR by BM3D-SAPCA image denoising," J. Lightwave Technol. **40**(24), 7952–7960 (2022).
21. J. Y. Yao, Y. H. Yao, F. Y. Cao, *et al.*, "Total variation and block-matching 3D filtering-based image reconstruction for single-shot compressed ultrafast photography," Opt. Lasers Eng. **139**(29), 106475 (2021).
22. P. Zdankowski, M. Trusiak, D. McGloin, *et al.*, "Quasi-noise-free stimulated emission depletion microscopy imaging of thick samples using adaptive optics and block-matching 3D filtering," in Imaging and Applied Optics (Optica Publishing Group, 2019), paper ITh1C.4.
23. J. A. Liang, Y. F. Guo, and B. Liu, "BM3D-based denoising method for color polarization filter array," Opt. Express **30**(12), 22107–22122 (2022).
24. A. Yang, Z. Ma, C. Zhang, *et al.*, "Review on application progress of federated learning model and security hazard protection," Digit. Commun. Netw. **9**(1), 146–158 (2023).
25. E. Francisca, R. Hurtado-Perez, M. Hernandez-Romo, *et al.*, "Digital image encryption using chaotic logistic mapping," in Frontiers in Optics (Optica Publishing Group, 2017), paper JTu2A.100.
26. J. Tian, L. Z. Yang, C. Qin, *et al.*, "Refractive index sensing based on chaotic correlation fiber loop ring down system using tapered fiber," IEEE Sensors J. **20**(8), 4215–4220 (2020).
27. W. J. Zeng, C. F. Zhang, X. S. Liang, *et al.*, "Chaotic phase noise-like encryption based on geometric shaping for coherent data center interconnections," Opt. Express **32**(2), 1595–1608 (2024).
28. Z. Yang, L. L. Yi, J. X. Ke, *et al.*, "Chaotic optical communication over 1000 km transmission by coherent detection," J. Lightwave Technol. **38**(17), 4648–4655 (2020).
29. T. W. Wu, C. F. Zhang, Y. H. Chen, *et al.*, "Compressive sensing chaotic encryption algorithms for OFDM-PON data transmission," Opt. Express **29**(3), 3669–3684 (2021).
30. Y. Q. Zhang, N. Jiang, A. K. Zhao, *et al.*, "Security enhancement in coherent OFDM optical transmission with chaotic three-dimensional constellation scrambling," J. Lightwave Technol. **40**(12), 3749–3760 (2022).
31. Z. Y. Hu, Z. Z. Chen, Y. M. Li, *et al.*, "Adaptive Transceiver Design for High-Capacity Multi-Modal Free-Space Optical Communications With Commercial Devices and Atmospheric Turbulence," J. Lightwave Technol. **41**(11), 3397–3406 (2023).
32. S. Malik and P. K. Sahu, "Assessment of the FSO communication system using adaptive and MIMO MPPM with pointing errors and an atmospheric turbulence channel," Appl. Opt. **60**(6), 1719–1728 (2021).
33. C. A. N. Santos, D. L. N. Martins, and N. D. A. Mascarenhas, "Ultrasound Image Despeckling Using Stochastic Distance-Based BM3D," IEEE Trans. on Image Process. **26**(6), 2632–2643 (2017).